International Journal of Numerical Methods for Heat & Fluid Flow

1353

Received 23 July 2025
Revised 10 November 2025
Accepted 13 December 2025

# Experimental and numerical study of up-down sloshing problems in rectangular tanks

Oscar González-Cofré and Marcela A. Cruchaga
*Departamento de Ingeniería Mecánica, Universidad de Santiago de Chile, Santiago de Chile, Chile*

Martin Lacroix, Eduardo Fernández and Jean-Philippe Ponthot
*Aerospatiale et Mecanique/LTAS-MN2L, Universite de Liege, Liege, Belgium, and*

Diego Celentano
*Departamento de Ingeniería Mecánica y Metalúrgica, Pontificia Universidad Catolica de Chile, Santiago, Chile*

## Abstract

**Purpose** – This paper aims to report an experimental and numerical study of sloshing in rectangular tanks subjected to vertical imposed motion.

**Design/methodology/approach** – The free-surface behavior of a fluid inside a rectangular tank subjected to imposed vertical motion is studied. The experiment consists of imposing motions to a rectangular tank mounted on a shake table controlled for vertical movements. The free surface is measured from images collected with high-speed cameras that record the sloshing experiments performed at different shaking frequencies. The numerical approach uses an algorithm based on the Particle Finite Element Method (PFEM) implemented in an in-house code. The time-periodic regime of the free-surface behavior is specifically studied. The numerical results are validated by comparison with the experimental data.

**Findings** – To allow a better comparison between experimental and numerical results, the time step used in the simulation should be shorter than that resulting from the sampling frequency of the recordings. To activate the mode shapes, the imposed frequency of the tank motion must be twice the natural frequency.

**Originality/value** – The novel aspects of this study include the experimental observation of free-surface mode-shapes through controlled vertically imposed motion, as well as the validation of the PFEM for this type of applications. The integration of experimental data, the use of a tailored numerical strategy and the validation of the numerical results constitute the original contributions of this work.

**Keywords** Fluid dynamics, Sloshing up-down, Experiments, PFEM numerical simulations

**Paper type** Research paper

## 1. Introduction

The phenomenon of sloshing, motion of a free surface of a fluid contained in a tank subjected to external accelerations, is highly relevant in numerous engineering applications. The dynamics of liquids in moving tanks have been extensively investigated in the context of

*Funding*: This study was supported by the Dirección de Investigación Científica y Tecnológica / Vicerrectoría de Investigación, Innovación y Creación/Universidad de Santiago de Chile project AYUDANTE DICYT Código 052516CSSA Grant Wallonie-Bruxelles International No. VII Commission AGCID-WBI RI07; Project TiNTHyN / Win4Excellence program – Project No. 2310142 from the Walloon Region Fondo Nacional de Desarrollo Científico y Tecnológico No. Fondecyt 1210228.

International Journal of Numerical Methods for Heat & Fluid Flow
Vol. 36 No. 3, 2026
pp. 1353-1377

0961-5539
DOI 10.1108/HFF-07-2025-0533

ground transportation (Grotle and Æsøy, 2018), marine vessels (Jiang *et al.*, 2015) and aerospace systems (Siraye *et al.*, 2023; Ayiehfor, 2024).

In the case of aerospace applications, understanding the motion of the free surface is crucial for the safe design and operation of onboard liquid storage tanks, such as those used for fuel or cryogenic propellants. When an aircraft undergoes acceleration – during takeoff, maneuvering, turbulence or landing – the interaction between the fluid and the tank walls can trigger resonance modes (Pizzoli *et al.*, 2023; Saltari *et al.*, 2022). If the imposed excitation frequency approaches one of the natural frequencies of the fluid–structure system, high dynamic pressures may arise, potentially affecting the stability, control or structural integrity of the vehicle.

The study of the sloshing phenomenon has been addressed through various numerical techniques, including the Finite Element Method (FEM) (Cruchaga *et al.*, 2013; Cruchaga *et al.*, 2016a; Battaglia *et al.*, 2018), Finite Volume Method (Jahanbakhsh *et al.*, 2007; Godderidge *et al.*, 2009; Caron *et al.*, 2018; Yang *et al.*, 2021), Particle Finite Element Method (PFEM) (Idelsohn *et al.*, 2004; Cremonesi *et al.*, 2020; Fernández *et al.*, 2023a), Smoothed Particle Hydrodynamics (SPH) (Rafiee *et al.*, 2011; Gotoh *et al.*, 2014; Cao *et al.*, 2019; Cai *et al.*, 2021), among others. Within the framework of each method, different strategies can be applied to describe the free surface. Some of these approaches use two-phase flow techniques, in which the interface between two working fluids – commonly water and air – needs to be explicitly described time by time. In (Cruchaga *et al.*, 2013) and (Battaglia *et al.*, 2018), finite element formulations were applied to simulate free-surface flows, whose numerical predictions were compared with experimental image-tracking data, demonstrating accurate results under various excitation conditions. In (Caron *et al.*, 2018) and (Battaglia *et al.*, 2018), these approaches were extended to three-dimensional and in (Battaglia *et al.*, 2022) Arbitrary-Lagrangian-Eulerian (ALE)-based configurations were used to improve interface tracking with mesh adaptation. In addition, (Cruchaga *et al.*, 2001) presented a moving-interface strategy for transient domains. Conversely, single-phase formulations proposed in (Cerquaglia *et al.*, 2019) and (Battaglia *et al.*, 2022) adopted a purely Lagrangian description, allowing direct tracking of the free surface without the need for a two-phase representation.

Several published studies address sloshing problems, but most focus on horizontal imposed motions, such as the experimental analysis in (Liu *et al.*, 2025), which examined primary and higher-mode resonance in a square-base tank under unidirectional excitation, and the combined numerical–experimental study in (Núñez Aedo *et al.*, 2024). Other works analyze rotational imposed motions, as in (Li *et al.*, 2024), where an adaptive SPH-based approach is employed for prismatic and rectangular tanks, validated through experimental and numerical results.

Studies on vertical sloshing are scarce in the literature, and it is even more difficult to find those that include both experimental and numerical aspects, even among the most recent ones. Experimental investigations such as those reported in (Pizzoli *et al.*, 2023; Saltari *et al.*, 2022) approach the problem through physical testing, with a focus on dissipation mechanisms and stability enhancement in aeronautical applications. Numerical studies, including (Zhang *et al.*, 2022), use the Moving Particle Semi-implicit method to reproduce free-surface evolution under vertical excitation, confirming the capability of particle-based schemes for this class of problems. Earlier works such as (Frandsen and Borthwick, 2003; Frandsen, 2004) also addressed vertically imposed motion through two-dimensional simulations in rectangular tanks using second-order finite difference formulations.

In addition to the numerical implementation used to solve the governing equations of motion, it is essential to validate the results using experimental data. Validation procedures

similar to those described in (Cruchaga *et al.*, 2016a) and (Li *et al.*, 2014) were adopted to ensure consistency between numerical and physical observations. In (Cruchaga *et al.*, 2009) and (Cruchaga *et al.*, 2016b), comparable methodologies were applied to free-surface problems in rectangular tanks, confirming the effectiveness of image-based measurements. Likewise (Battaglia *et al.*, 2022), analyzed similar geometries and flow conditions, although under horizontally imposed excitations. These studies are particularly relevant, as they use tanks with the same geometric parameters as those used in the present study.

In particular, the present work investigates the response of the free surface at different frequencies corresponding to the first mode shapes in a tank with an aspect ratio of 2:1. Experimental data are obtained following procedures such as those described in (Cruchaga *et al.*, 2013; Castillo *et al.*, 2019; Núñez Aedo *et al.*, 2020). The numerical study focuses on two-dimensional (2D) cases, using the PFEM to solve the free-surface problem, incorporating an Alpha-shape-based remeshing technique (Idelsohn *et al.*, 2004; Fernández *et al.*, 2023a; Fernández *et al.*, 2023b). The core focus of this work is the experimental validation of the PFEM-based numerical model. Despite extensive studies on horizontally and rotationally induced sloshing, experimental evidence on vertically excited sloshing and its validation through numerical particle-based methods remains scarce. In particular, the application of the PFEM to vertical sloshing problems has not been previously reported. The novelty of this work lies in the experimental observation of vertical sloshing mode shapes, which have been scarcely reported, and the validation of PFEM for vertically induced free-surface oscillations. The combination of synchronized high-speed imaging and a remeshing-based Lagrangian solver provides a unique framework to analyze sloshing modes under vertical excitation.

Summarizing the original contents of this work are:

- Report a new experimental work to reproduce vertical induced motions.
- Modeling using a PFEM framework not previously applied to this problem.
- Emphasis on exhaustive validation of the proposed numerical method by comparison with the experimental data.

This paper is structured as follows. The experimental work conducted is reported in Section 2. The numerical method used and the corresponding model description are presented in Section 3. The comparison between experimental and numerical results can be found in Section 4. Finally, the conclusions are drawn.

## 2. Experimental work

### *2.1 Experimental setup*

The experimental setup consists of a transparent acrylic rectangular tank, with an aspect ratio of 2:1 ($L/W$), mounted on a shake table modified to perform controlled vertical motion. The dimensions of the tank are indicated in Figure 1, with $L = 400\,mm$, $W = 200\,mm$ and $H = 490\,mm$. The shake table is driven by a motor that generates horizontal displacement via a power screw, with the direction change between the screw and the platform achieved through a scissor lift mechanism. Accelerations of up to $2.5\,g$ can be applied. The imposed acceleration depends on the load applied to the table. The maximum admissible force is $500\,N$ at reduced acceleration. In the present experiment the maximum admissible acceleration is $1.8\,g$ considering the self-weight of the mechanism.

To capture the free-surface behavior, two high-speed cameras are positioned perpendicularly to the tank faces, CAM1 at front face and CAM2 at the lateral face, as shown in Figure 1, enabling simultaneous tracking from both sides. A vertical imposed motion of

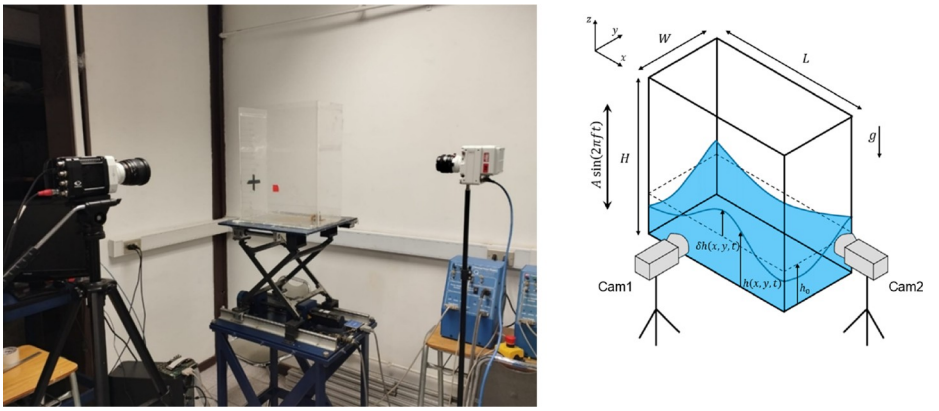


**Figure 1.** Experimental set-up: laboratory layout (left), tank geometry and position of the cameras (right)

the form $z = A\sin(2\pi ft)$ is applied during the tests, with amplitude $A = 1.5\,mm$ and imposed frequency $f_{ij}$ depending on the mode shape to be excited. Figure 1 shows the experimental setup located at the Laboratory of Vibrations and Fluid-Structure Interaction, Department of Mechanical Engineering, University of Santiago of Chile.

In the case of vertically imposed motion, it is important to note that the gravitational acceleration acts in the same direction as the imposed excitation. As a result, when the problem is considered in a relative reference frame, the tank experiences alternating periods in which the effective acceleration exceeds or falls below the gravitational acceleration. Figure 2 illustrates this behavior associated with the imposed vertical movement in the tank in a single cycle with period *T*.

During one complete cycle of free-surface motion in the time-periodic regime, two full cycles of motion of the shake table must occur. Figure 2 shows the evolution of the free surface throughout two consecutive cycles of platform oscillation.

It can be seen that when the platform reaches the uppermost point of its trajectory, the free surface is fully compressed against the bottom of the tank. This corresponds to the instant of maximum acceleration in the same direction as gravity (maximum effective gravity). In contrast, when the platform is at the lowest point of its stroke, the wave height reaches its

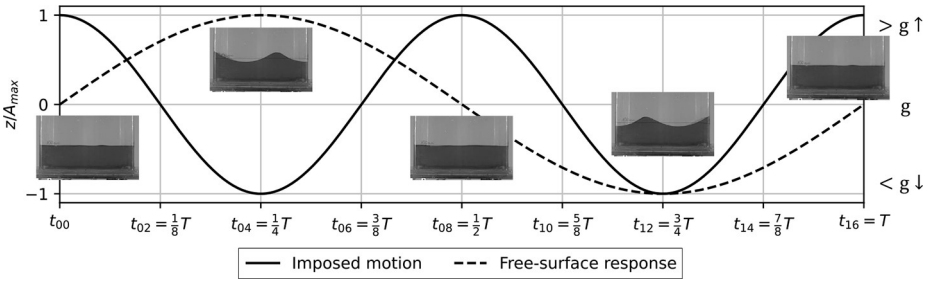


**Figure 2.** Tank behavior for vertical motion

maximum, indicating a moment of acceleration in the opposite direction to gravity (reduced effective gravity).

This sequence repeats due to the physical characteristics of the wave motion, producing alternating phases of high and low effective gravity acting on the tank, thereby completing one full cycle of the free-surface behavior of the fluid.

The analytical natural frequencies $f_{ij}$ for sloshing in a rectangular tank are obtained as reported by (Battaglia *et al.*, 2018; Ibrahim, 2005), $f_{ij}^2 = g\ k_{ij}\ tanh(k_{ij}h_0)/(4\pi^2)$, where $g$ is the gravity; $k_{ij} = \pi\sqrt{\frac{i^2}{L^2} + \frac{j^2}{W^2}}$ with $i$ and $j$ being the indices associated with the activation of the mode shape in the $x-$ and $y-$ direction of the tank, respectively; and $h_0$ is the fill depth, 100 *mm* of water in the present analysis. For the purposes of this study, the analysis is focused on the frequencies corresponding to the first seven mode shapes. Note that the analytical expression used to estimate the natural frequencies of the fluid does not depend on the direction of the imposed motion. Instead, this is solely determined by the geometric characteristics of the tank, the depth of the fluid and the gravitational acceleration of the system. Table 1 presents the natural frequencies associated with each mode under consideration, as well as the experimentally imposed excitation frequency used for vertical motion.

### *2.2 Procedure for recollecting the experimental data*

The procedure for experimental data collection is based on image tracking from high-speed cameras arranged as shown in Figure 1. For CAM1 (front view), a Phantom LAB MIRO M110 camera is used, with a maximum sampling rate of 1600 $fps$ at full resolution (1280 × 800 $px$). For CAM2 (side view), a Phantom VEO-E 310 L camera is employed, with a maximum sampling rate of 3200 $fps$ at full resolution (1280 × 800 $px$). Both cameras are used in monochrome configuration and can be synchronized to trigger simultaneously, allowing for simultaneous capture of both views of the experiment. The image acquisition frequency used in this study is 100 $fps$, which ensures smooth tracking of the free-surface behavior.

The captured images are processed using a superimposed grid to define the physical dimensions of the tank. For CAM1, a grid of 400 × 200 $mm$ with 10 × 10 $mm$ cells is used, covering the full width of the front face ($L = 400\ mm$), resulting in a measurement scale of 2.95 $px/mm$ and an associated error of $\pm 0.68\ mm$. For CAM2, a grid of 200 × 200 $mm$ with 10 × 10 $mm$ cells is applied across the width of the lateral face ($W = 200\ mm$), with a scale of 3.5 $px/mm$ and an associated error of $\pm 0.57\ mm$. These grids enable the tracking of the free-surface behavior in contact with the tank walls. Figure 3 shows the grid configuration overlaid on the images captured by CAM1 and CAM2.

For every case defined according to the imposed frequencies previously detailed in Table 1, specific control points (CPs) are adopted to capture the free-surface behavior, where the wave height is tracked over time from the recorded images. Figure 4 shows the spatial

**Table 1.** Natural and experimentally imposed frequencies *[Hz]* for 3D behavior at the first Seven mode shapes

| Modes | $i$<br>$j$ | 1<br>0 | 2<br>0 | 0<br>1 | 1<br>1 | 2<br>1 | 3<br>0 | 3<br>1 |
|---|---|---|---|---|---|---|---|---|
| Analytical natural frequency | | 1.16 | 1.93 | 1.97 | 2.09 | 2.38 | 2.44 | 2.70 |
| Experimental imposed frequency | | 2.32 | 3.86 | 3.94 | 4.18 | 4.76 | 4.88 | 5.40 |

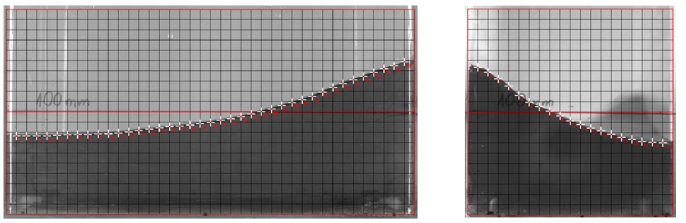

**Figure 3.** Procedure for capturing wave height

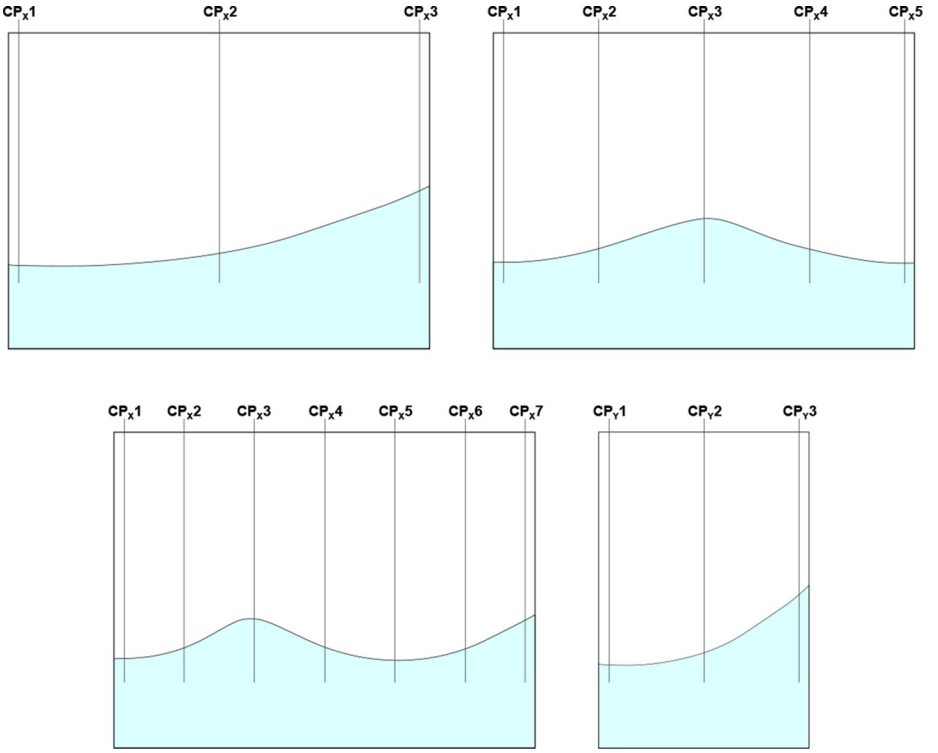


**Figure 4.** Location of control points along the front and lateral (bottom row, right figure) faces of the tank, from now on the CPs on the front face will be called as $CP_x$ and $CP_y$ for the three CPs on the lateral face

configuration of the CPs within the tank for each mode shape. Table 2 lists the exact position of each CP on the front face of the tank for each of the analyzed cases.

For the lateral face, the configuration of the CPs is similar to that defined for the first mode on the front face of the tank, with the only difference being their spatial location along the lateral side. Table 3 presents the positions of the CPs on the lateral face.

**Table 2.** Location [mm] of control points CPs along the front face ($x$ – direction) of the tank, configuration for each studied sloshing mode

| CP | 1st | 2nd | 3rd |
|---|---|---|---|
| $CP_X1$ | 10 | 10 | 10 |
| $CP_X2$ | 200 | 100 | 66.7 |
| $CP_X3$ | 390 | 200 | 133.3 |
| $CP_X4$ | | 300 | 200 |
| $CP_X5$ | | 390 | 266.7 |
| $CP_X6$ | | | 333.3 |
| $CP_X7$ | | | 390 |

**Table 3.** Location [mm] of control points CPs along the lateral face ($y$ – direction) of the tank

| CP | 1st |
|---|---|
| $CP_Y1$ | 10 |
| $CP_Y2$ | 100 |
| $CP_Y3$ | 190 |

For the cases that can be considered two-dimensional – i.e. those in which either index i or j is equal to zero – the CP configuration is assumed to be the same as that used for the first mode in the previously defined setups, on the face where the behavior is planar.

*2.3 Experimental results analysis*

Experimentally, six case studies are analyzed, corresponding to the first natural frequencies. Each experimental case was repeated three times and it was verified that the difference between those measurements is limited to the experimental error, which verifies the repeatability of the observations. The cases corresponding to imposed frequencies of 2.32 *Hz*, 3.86 *Hz* and 4.88 *Hz* exhibit bidimensional behavior on the front face of the tank. The case with imposed frequency of 3.94 *Hz* is also bidimensional but on the lateral face of the thank; therefore, it is not analyzed in the present study. As an example, Figure 5 illustrate a typical 2D behavior of the free surface associated to frequency $f_{10}$. The mode clearly appears on the frontal wall and, approximately extends to the back of the tank as shown the flat evolution of the free surface on the lateral face. Snapshots and the evolution of the free surface for these kind of cases are reported in Section 4 together with the numerical results for comparison proposal.

The remained three studied cases exhibit fully three-dimensional (3D) behavior, associated with the imposed frequencies of 4.18 *Hz*, 4.76 *Hz* and 5.40 *Hz*. In these cases, a combination of the first three modes shape on the front face and the first mode shape on the lateral face is observed, see Figures 6–8, respectively. The experimental free-surface evolutions obtained for those 3D cases at certain CPs are presented for a given time interval within the time-periodic regime in Figures 9(a), 10(a) and 11(a) for the register at the front face and Figures 9(b), 10(b) and 11(b) for the register at the lateral face of the tank.

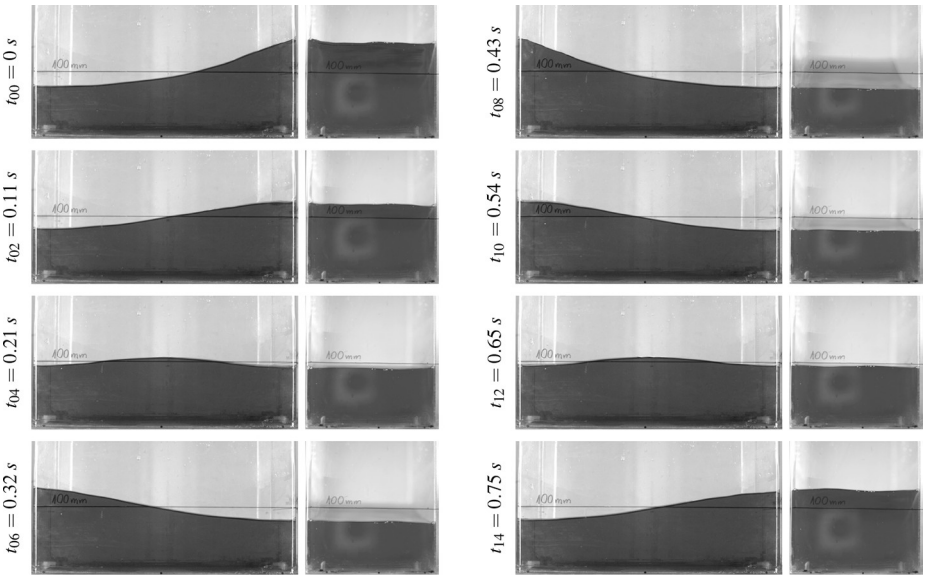


**Figure 5.** Experimental free-surface behavior at 2.32 *Hz*: front (left) and lateral (right) in each column

## 3. Numerical work

This section presents the model used for the numerical study of up-down sloshing problem, and the numerical simulation of the problem made in the context of the PFEM (Idelsohn *et al.*, 2004; Cremonesi *et al.*, 2020; Fernández *et al.*, 2023a; Cerquaglia *et al.*, 2019; Fernández *et al.*, 2023b; Oñate *et al.*, 2004; Idelsohn *et al.*, 2014; Gimenez *et al.*, 2017). For completeness, a short description of the method is included.

### *3.1 Governing equations and particle finite element method*

In simple terms, the PFEM consists of two main steps during each time step of the simulation of dynamic problems. The first step involves solving the governing equations in a *Lagrangian framework* using the FEM, through which the nodal states and positions are computed. The second step corresponds to *remeshing* the fluid domain based on predefined mesh quality criteria.

This study considers incompressible Newtonian fluids. The continuous model solved by the PFEM algorithm involves the Navier–Stokes equations, written as:

$$\rho \frac{d\mathbf{v}}{dt} - \mu \Delta \mathbf{v} + \nabla p = \mathbf{f} \tag{1}$$

$$\nabla \cdot \mathbf{v} = 0 \tag{2}$$

where $\rho$ is the fluid density, $d/dt$ denotes the Lagrangian time derivative, $t$ is time, and $\mathbf{v}$ is the velocity vector. The constitutive behavior of Newtonian fluids is described by the dynamic viscosity $\mu$ and the pressure $p$. The vector of external forces is represented by $\mathbf{f}$.

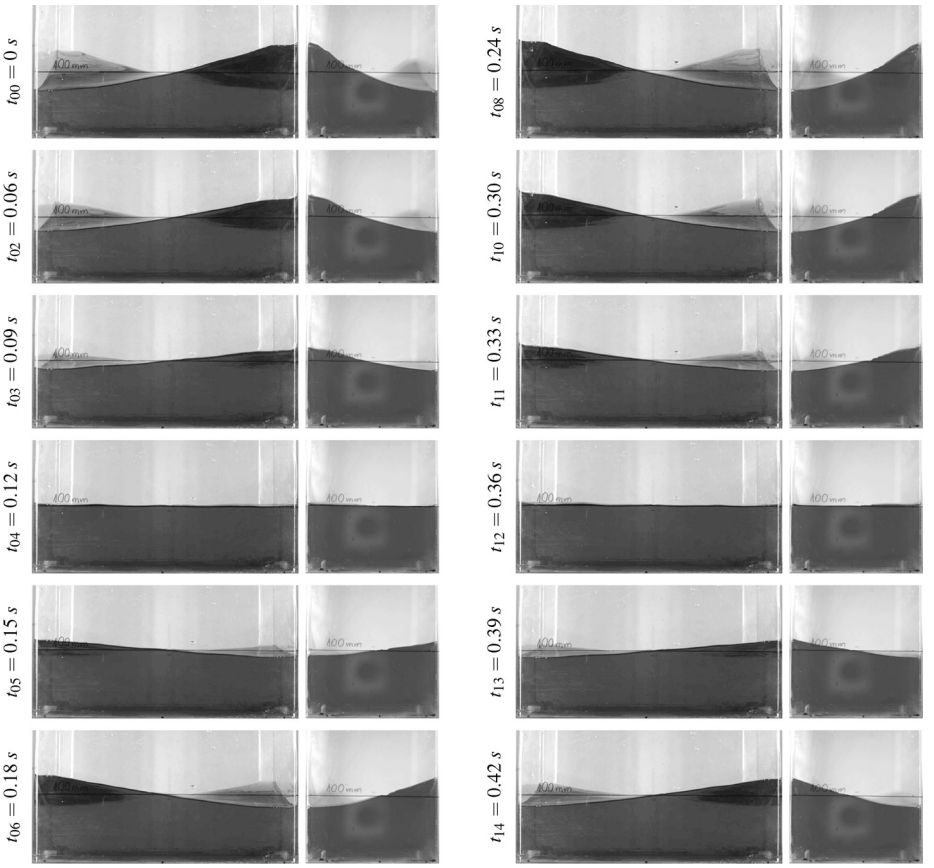


**Figure 6.** Experimental free-surface behavior at 4.18 *Hz*: front (left) and lateral (right) in each column

The equations are spatially discretized using a FEM–Galerkin formulation with a pressure-stabilizing Petrov–Galerkin (PSPG) stabilization technique is employed to enhance numerical stability (Fernández *et al.*, 2023a; Cerquaglia *et al.*, 2019). The time discretization is performed using a backward Euler scheme. In this study, a user-defined criterion is defined to fix the time step. The iterative procedure begins with a specified initial time step, $\Delta t = 0.001$ s in the present study. After that, the time step is adjusted as follows: if convergence is not achieved, it is divided by 2; otherwise, if there are no convergence problems, it is multiplied by 1.5. In addition, the time step can increase up to a maximum value, set equal to the initial time step.

Remeshing is performed using Delaunay triangulation combined with the alpha-shape criterion, with an upper bound for alpha of 1.2, as commonly reported in the PFEM literature (Idelsohn *et al.*, 2004; Cremonesi *et al.*, 2020; Fernández *et al.*, 2023a). In addition to the *alpha-shape* algorithm, two commonly used criteria are also considered for the remeshing step of PFEM. Because nodes move according to the equations of motion, if the distance between two nodes becomes smaller than $\gamma h_u$, one of the nodes is removed from the model.

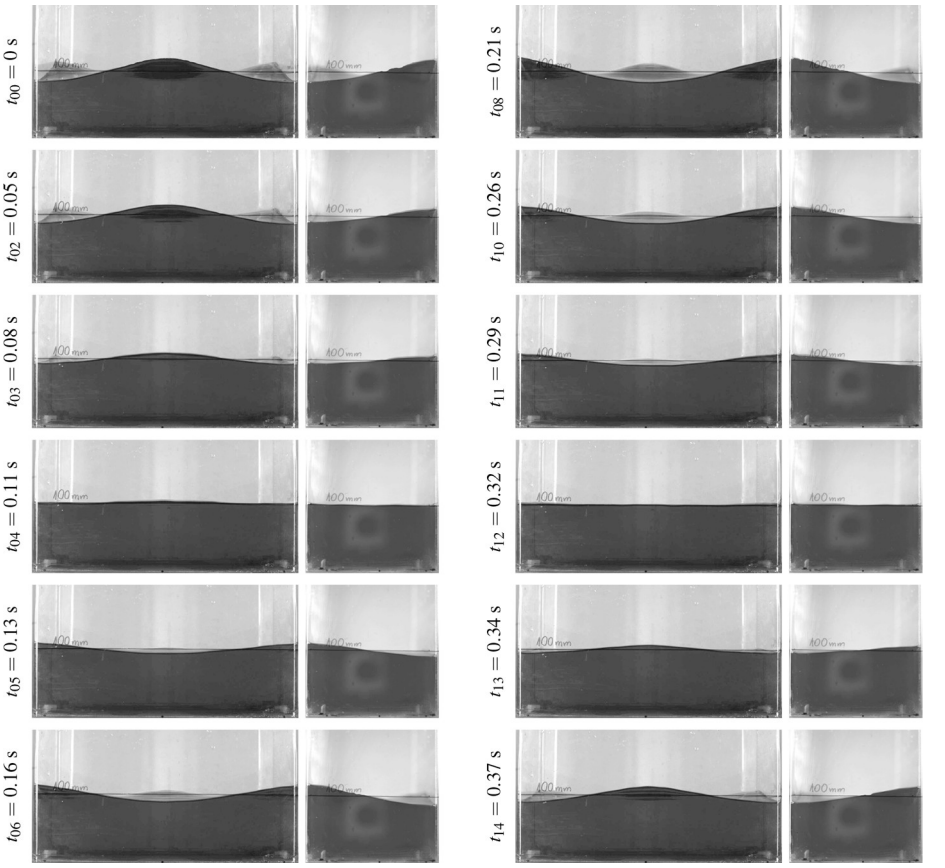


**Figure 7.** Experimental free-surface behavior at 4.76 *Hz*. front (left) and lateral (right) in each column

Conversely, if the area of an element exceeds $\omega h_u^2$, a new node is inserted at the centroid of the element. Where $h_u$ is the user-defined characteristic element size, and $\gamma$ and $\omega$ are tuning parameters numerically setting to avoid excessive loss or gain of mass (Fernández *et al.*, 2023a). Advanced remeshing techniques were proposed in the literature for improving the mass conservation within the PFEM framework (Fernández *et al.*, 2023a; Falla *et al.*, 2023). In addition, the present version of PFEM enables the description of surface-tension ($\sigma$) effects following the reports given in (Cerquaglia *et al.*, 2019; Yvonnet *et al.*, 2008; Fernández *et al.*, 2024).

### *3.2 Numerical model*

The numerical model is used to simulate the experimental setting presenting two-dimensional modes only. These cases correspond to the frequencies $f_{1,0}$, $f_{2,0}$, $f_{3,0}$ and $f_{4,0}$, which exhibit 2D behavior on the front face of the tank, and $f_{0,1}$, which shows 2D behavior on the lateral face.

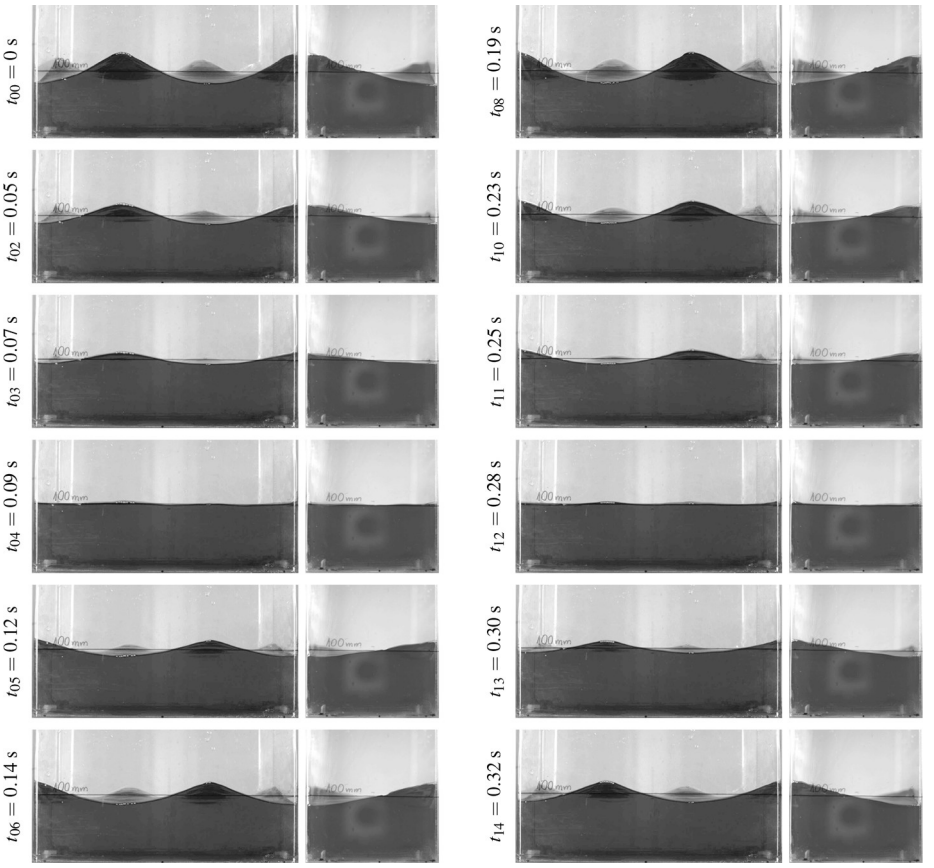


**Figure 8.** Experimental free-surface behavior at 5.40 $Hz$: front (left) and lateral (right) in each column

The mesh used for the numerical simulations consists of triangular elements, which is a requirement for the remeshing process of PFEM. Figure 12 illustrates the initial mesh. A nonuniform element size is defined in the model, with $h_u = 2\,mm$ in the free-surface region, and $h_u = 7\,mm$ in the bottom of the tank. A linear interpolation defines $h_u$ in between. The numerical method uses a single-phase fluid approach; therefore, only the water domain is meshed. The physical properties used in the simulation are $\rho = 1000\,kg/m^3$, $\mu = 0.001\,Pa \cdot s$ and $\sigma = 0.072\,N/m$. The Alpha-shape parameter is set to $\alpha = 1.2$ for large elements, and the tuning parameters are $\omega = 0.7$ and $\gamma = 0.3$. A special consideration is applied when the nodes belong to the free surface, in which case the parameter $\gamma_{FS} = 0.2$ (Fernández *et al.*, 2023a).

## 4. Numerical validation: comparison with the experimental data

This section shows the numerical-experimental comparison of the results obtained for sloshing problem with vertical imposed motion. Digital CPs are used, following the same spatial arrangement as in the experimental free-surface tracking. Figures 13(a) and (b), 14(a) and (b) and 15(a) and (b) show the free-surface behavior and the frequency response spectra

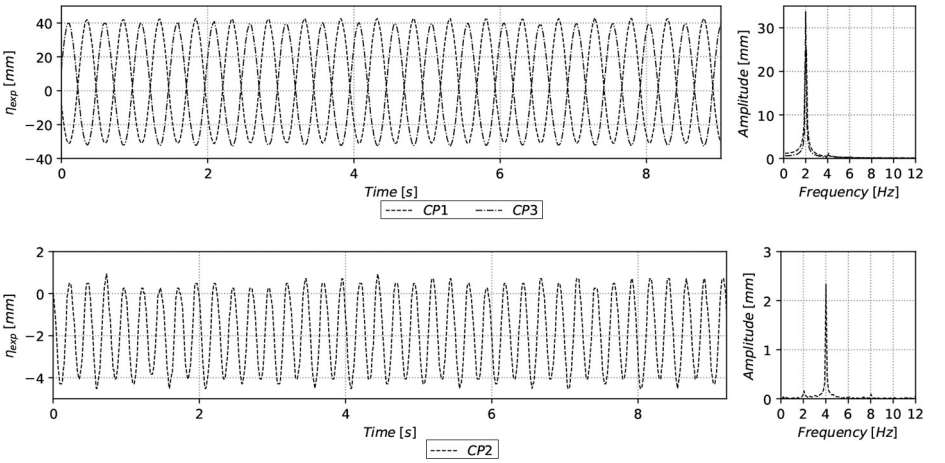


**(a)** Experimental behavior at 4.18 $Hz$ in front face

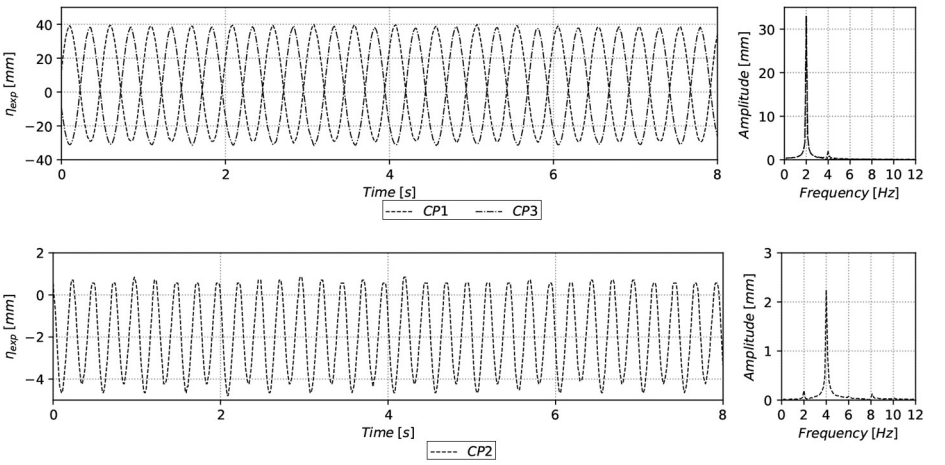


**(b)** Experimental behavior at 4.18 $Hz$ in lateral face

**Figure 9.** Experimental behavior at 4.18 $Hz$ of CPs (left) and FFT spectrum (right)

at the CPs shown in Figure 4 and listed in Table 2. These figures show a good correlation of the numerical results [Figures 13(b), 14(b) and 15(b)] with respect to the experimental ones [Figures 13(a), 14(a) and 15(a)]. However, particularly for the higher frequencies, the evolution of the free surface at points located $CP_X2$, $CP_X4$, $CP_X6$ which record lower amplitudes, differs more from its experimental counterpart. To explain these differences, we evaluated the mass lost or gained in the simulation, which is a well-known source of errors in PFEM (Idelsohn *et al.*, 2004; Cremonesi *et al.*, 2020). Figures 16(a), 17(a) and 18(a) show the mass evolution during the analyses. The initial total mass is 40 $kg$ per meter of thickness. The figures show that mass can be created or reduced due to the addition or removal of elements during the standard alpha-shape remeshing process, even when appropriate

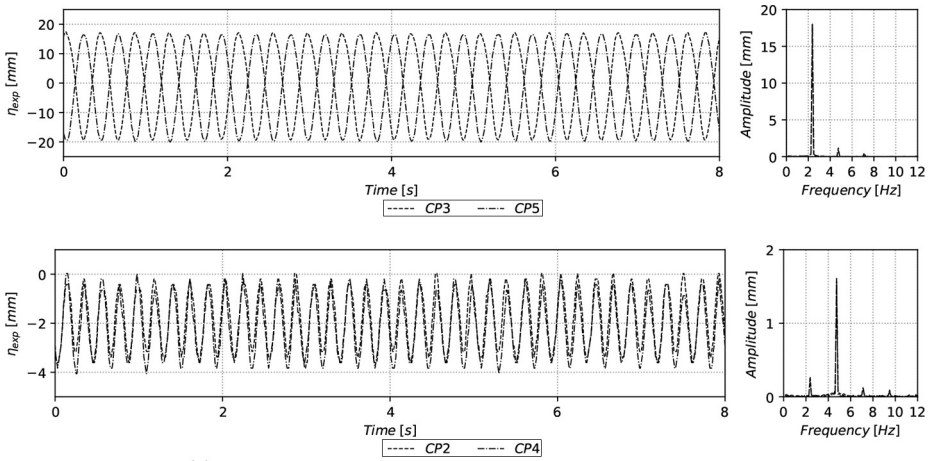


**(a)** Experimental behavior at 4.76 $Hz$ in front face

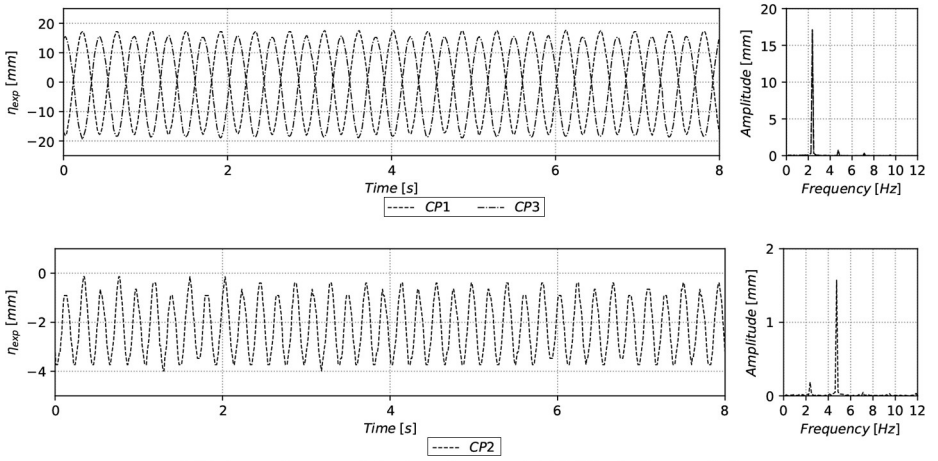


**(b)** Experimental behavior at 4.76 $Hz$ in lateral face

**Figure 10.** Experimental behavior at 4.76 $Hz$ of CPs (left) and FFT spectrum (right)

adjustments of the alpha-shape parameters, $\gamma$ and $\omega$ are made to reduce that variation. To overcome this fact, in the present work, a mass correction is applied as a post process to the computed free-surface evolution. This correction consists of shifting the free surface vertically according to the difference between the current mass and the original mass. The corrected free-surface evolution are plotted in Figures 16(b), 17(b) and 18(b). It can be seen that these figures improve the predictions of the evolution of the free surface.

Snapshots for experiments and simulations at different instants are plotted in Figures 19–21, globally confirming the good behavior of numerical simulations.

Finally, Figures 22–24 show a zoom of the experimental and numerical free-surface evolutions, a good fit is also observed in such a figures.

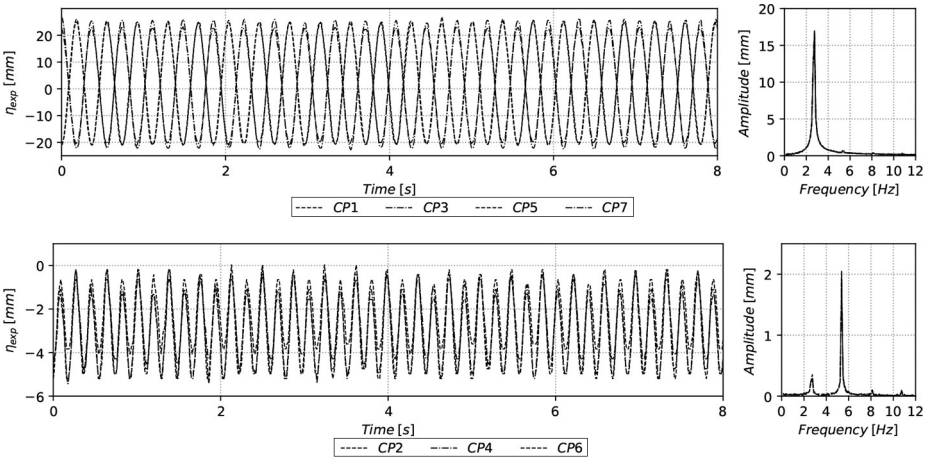


**(a)** Experimental behavior at 5.40 $Hz$ in front face

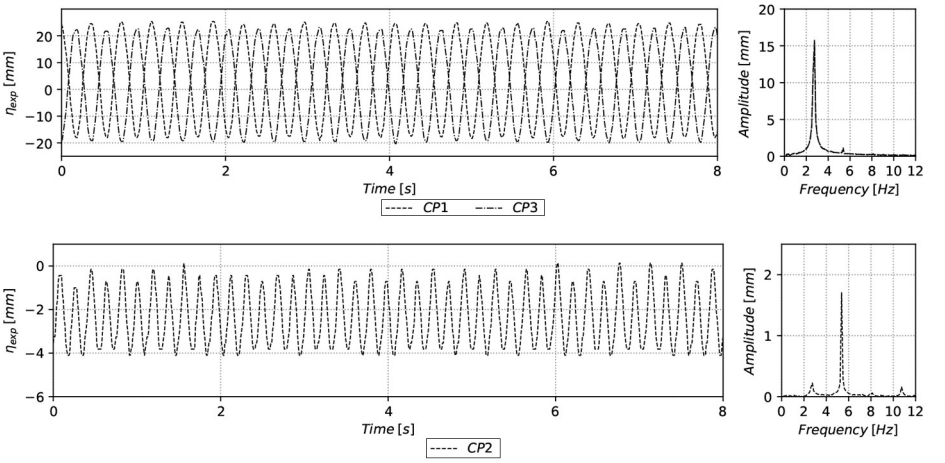


**(b)** Experimental behavior at 5.40 $Hz$ in lateral face

**Figure 11.** Experimental behavior at 5.40 $Hz$ of CPs (left) and FFT spectrum (right)

Table 4 reports the frequencies present in the experimental and numerical free-surface responses at the given CPs. The relative error of the dominant frequency of those responses is computed as $\varepsilon_r = |f - \overline{f}|/\overline{f} \times 100$, with respect to $\overline{f}$ taken as the analytical natural (reported in column 2 of such a table) or imposed (reported in column 3) frequencies, depending on the case, for each of the analyzed mode shapes. As observed, the frequencies of the free surface correspond both to the natural frequency and to the imposed excitation frequency applied to the tank.

Table 5 show the maximum and minimum wave heights $\eta$ for the experimental and numerical studies. The reported values are average of maximum (or minimum) during a representative time interval. The error is the standard deviation for the collection of

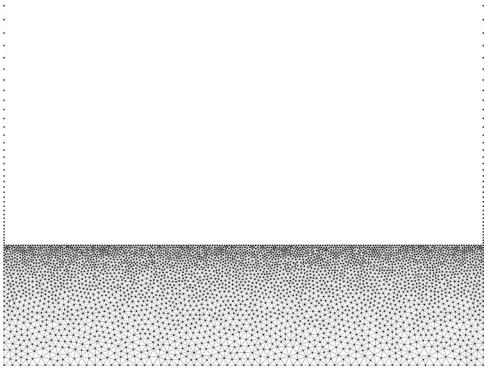

**Figure 12.** Initial mesh used in the numerical simulation

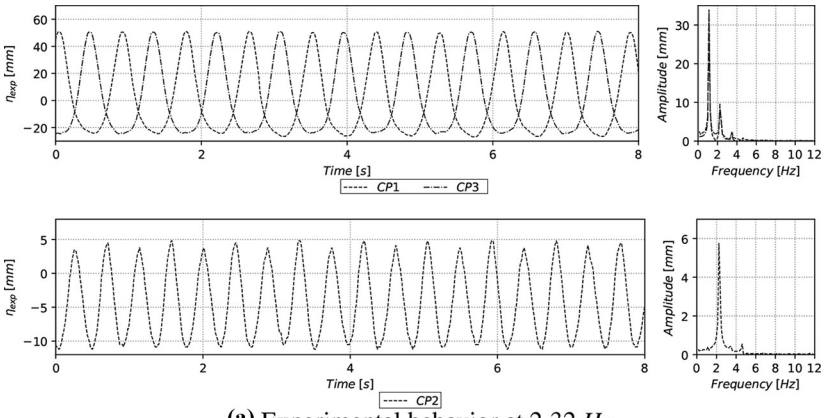


**(a)** Experimental behavior at 2.32 $Hz$

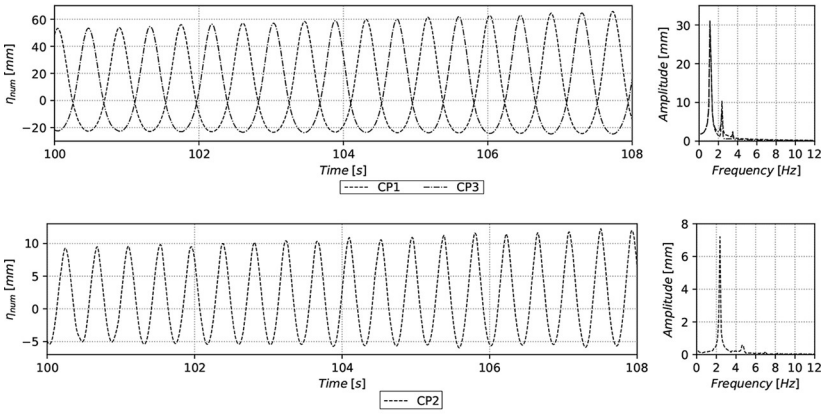


**(b)** Numerical behavior at 2.32 $Hz$

**Figure 13.** Experimental (a) and numerical (b) behavior at 2.32 $Hz$ of CPs (left) and FFT spectrum (right)

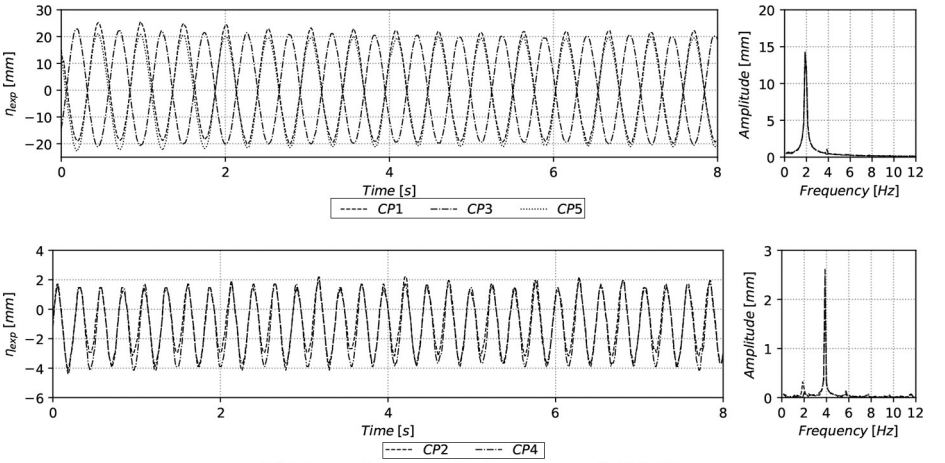


**(a)** Experimental behavior at 3.86 $Hz$

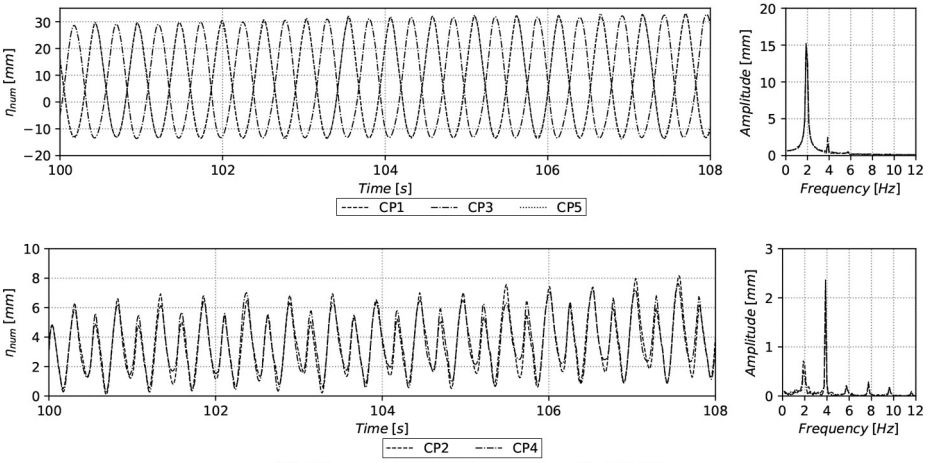


**(b)** Numerical behavior at 3.86 $Hz$

**Figure 14.** Experimental (a) and numerical (b) behavior at 3.86 $Hz$ of CPs (left) and FFT spectrum (right)

maximums (or minimums) values. These results confirm a good fit between numerical predictions and experiments.

## 5. Concluding remarks

This work investigates vertical up-and-down sloshing through both experimental and numerical approaches. The experiment considers a rectangular tank filled with water and subjected to vertical excitation at three different frequencies, aiming to excite the first

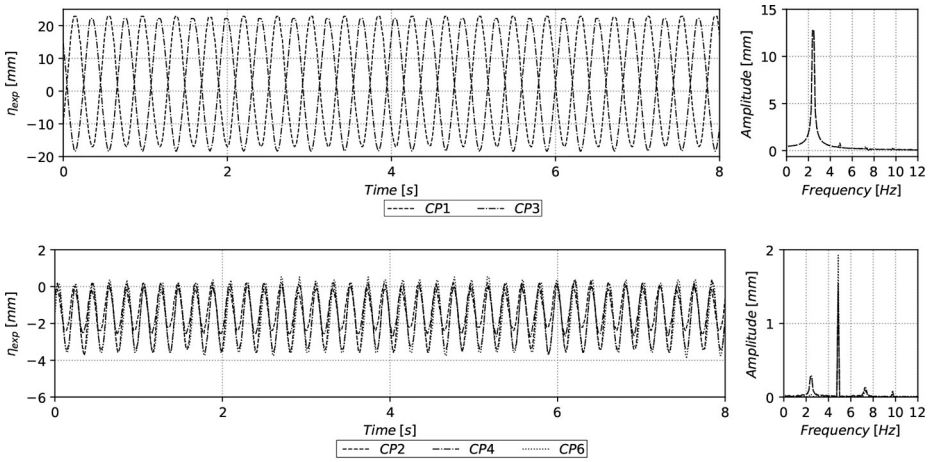


**(a)** Experimental behavior at 4.88 $Hz$

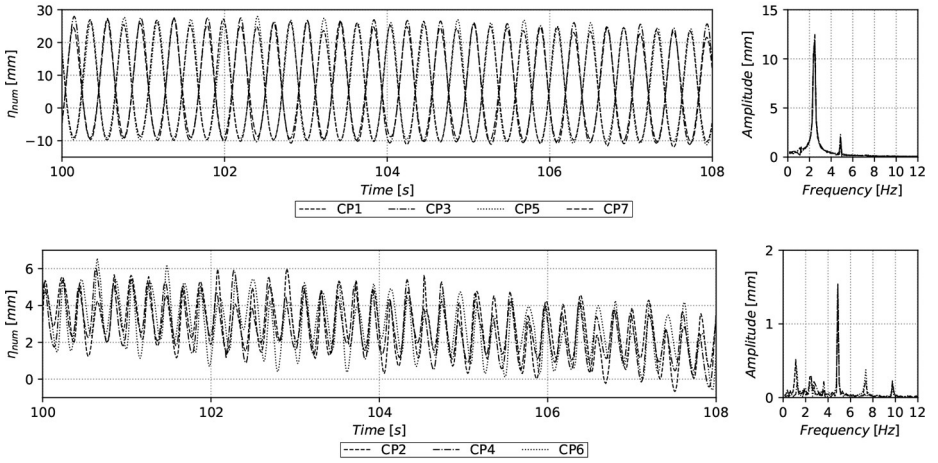


**(b)** Numerical behavior at 4.88 $Hz$

**Figure 15.** Experimental (a) and numerical (b) behavior at 4.88 $Hz$ of CPs (left) and FFT spectrum (right)

sloshing modes. PFEM is used to simulate, in 2D, the experimental setup that leads to two-dimensional sloshing modes.

The numerical and experimental results show agreement in both amplitude and frequency, allowing the validation of PFEM for vertical sloshing simulations. The maximum absolute error between numerical and experimental values reaches 0.11 Hz for frequencies and 5 mm for wave heights after applying the mass correction. In addition, we show that mass variation, a well-known source of error in PFEM, affects the sloshing modes. However,

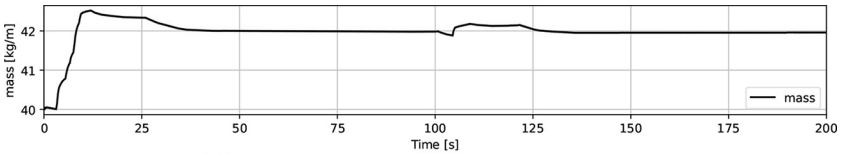


**(a)** Numerical mass behavior at 2.32 $Hz$

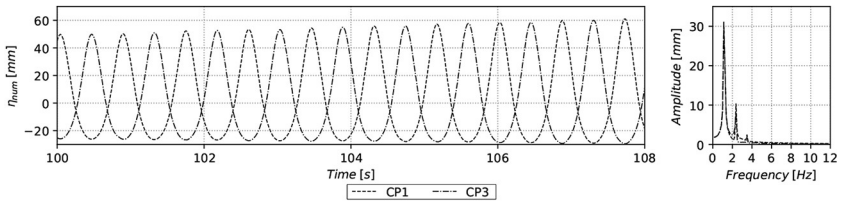


**(b)** Numerical behavior at 2.32 $Hz$ with mass correction

**Figure 16.** Mass evolution at 2.32 $Hz$ (a) and numerical free-surface evolution at CPs with external mass correction (b)

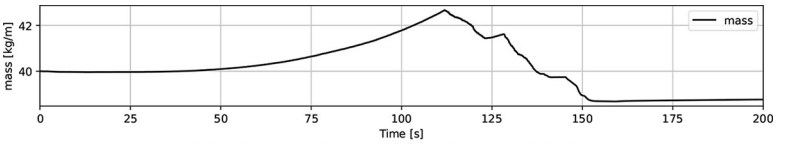


**(a)** Numerical mass behavior at 3.86 $Hz$

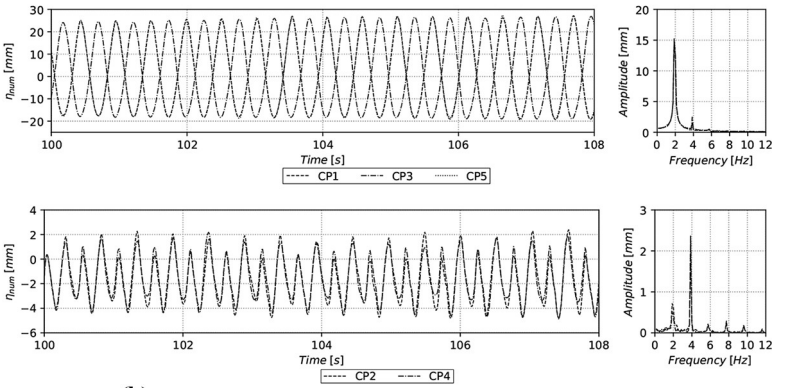


**(b)** Numerical behavior at 3.86 $Hz$ with mass correction

**Figure 17.** Mass evolution at 3.86 $Hz$ (a) and numerical free-surface evolution at CPs with external mass correction (b)

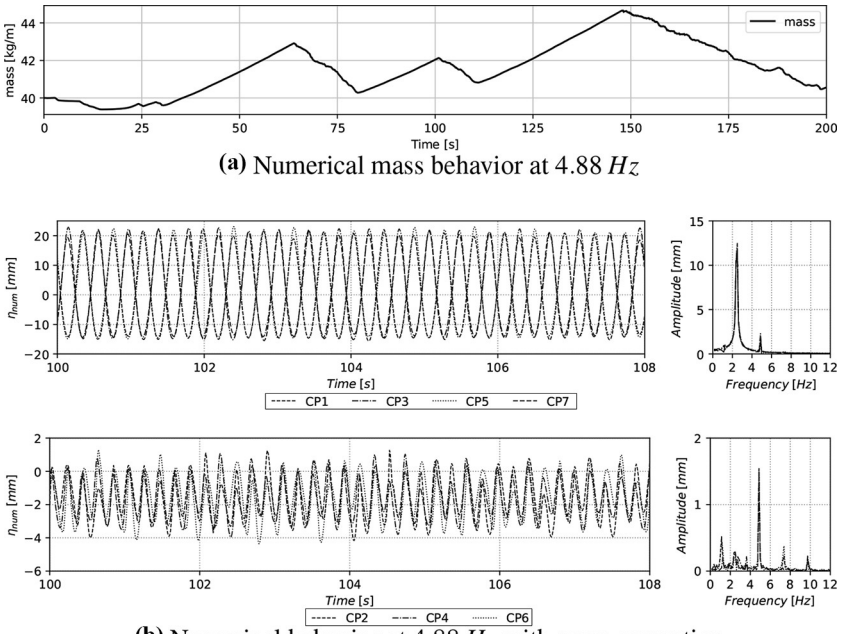


**(a)** Numerical mass behavior at 4.88 $Hz$

**(b)** Numerical behavior at 4.88 $Hz$ with mass correction

**Figure 18.** Mass evolution at 4.88 $Hz$ (a) and numerical free-surface evolution at CPs with external mass correction (b)

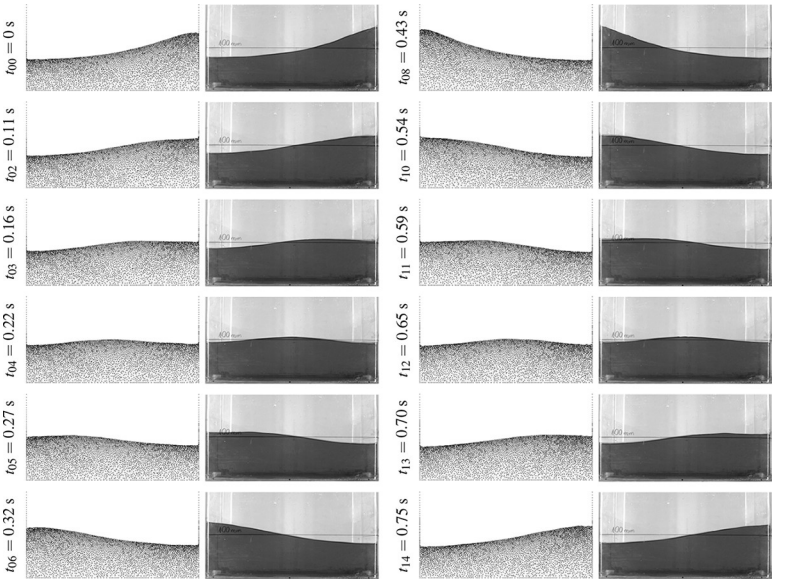


**Figure 19.** Free-surface behavior at 2.32 $Hz$: Numerical (left), Experimental (right)

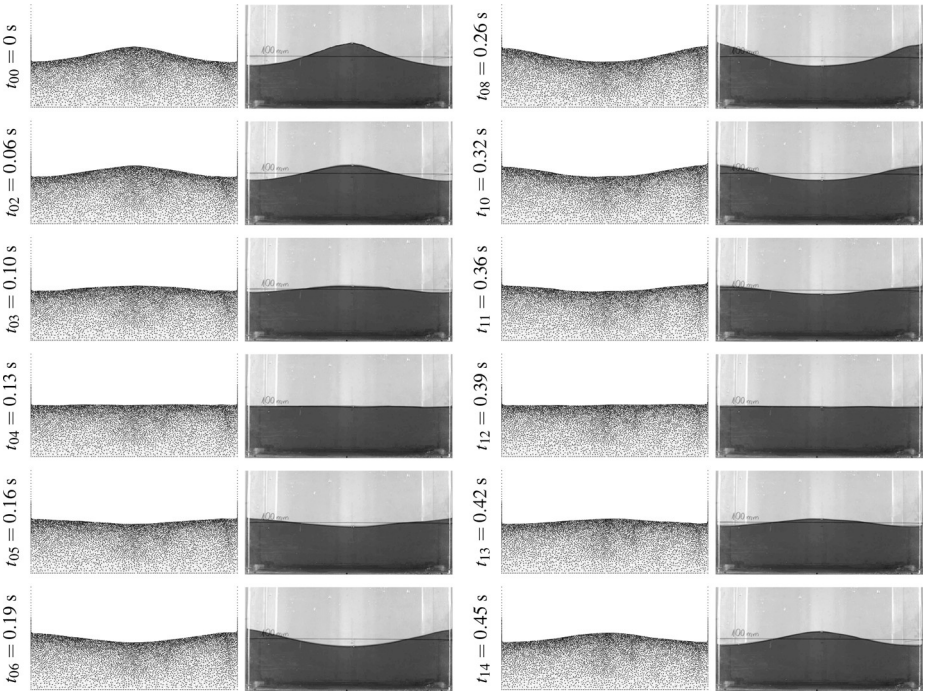


**Figure 20.** Free-surface behavior at 3.86 *Hz*: Numerical (left), Experimental (right)

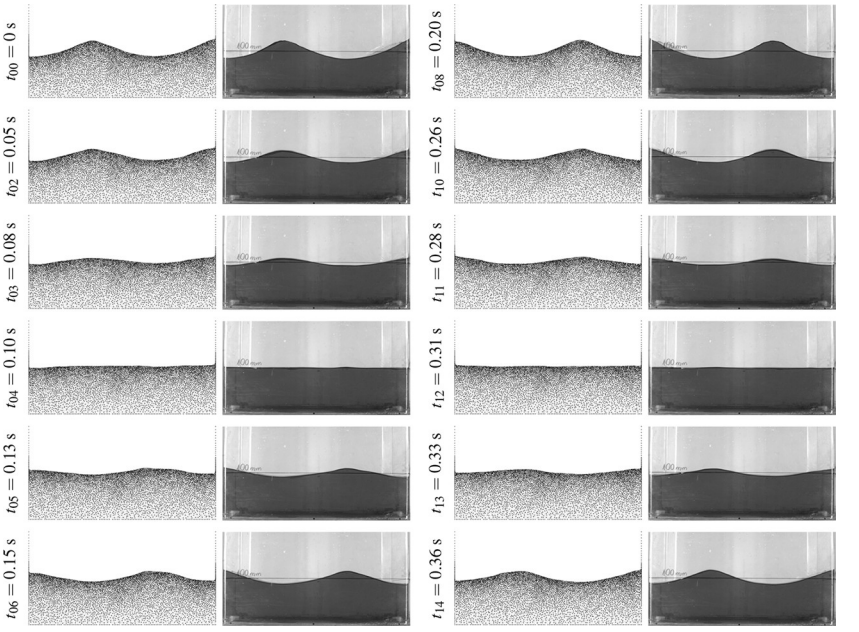


**Figure 21.** Free-surface behavior at 4.88 *Hz*: Numerical (left), Experimental (right)

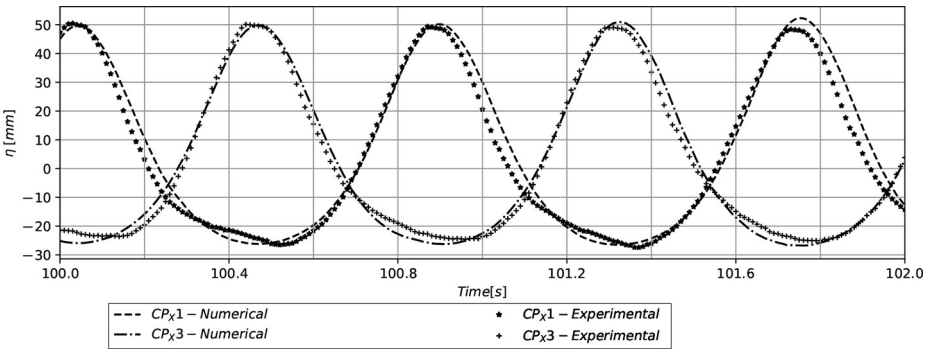


**Figure 22.** Comparison between numerical and experimental results for CPs at 2.32 $Hz$

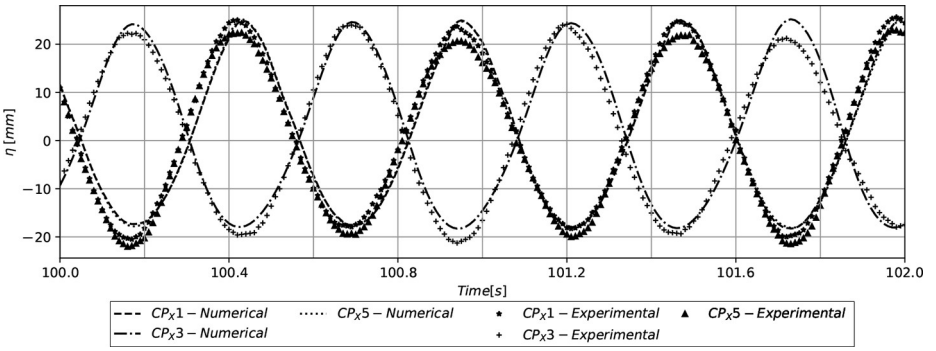


**Figure 23.** Comparison between numerical and experimental results for CPs at 3.86 $Hz$

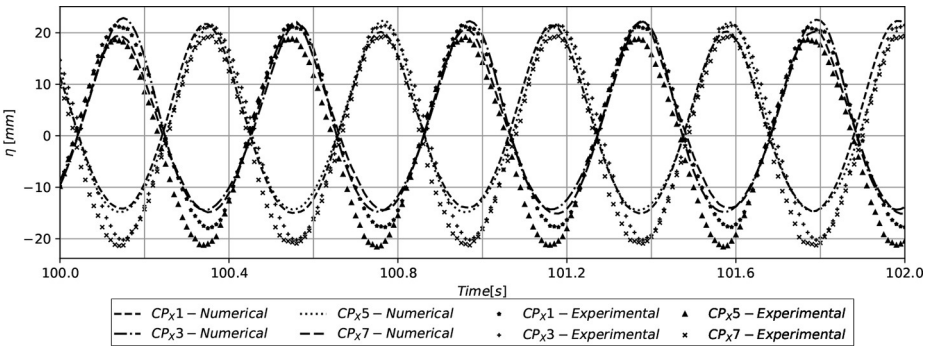


**Figure 24.** Comparison between numerical and experimental results for CPs at 4.88 $Hz$

**Table 4.** Comparison of frequencies in *[Hz]* for sloshing responses

| $f_{ij}$ | Analytical natural frequency | Imposed frequency | CP | Frequency Exp. | Frequency Num. | Relative error* Exp. | Relative error* Num. |
|---|---|---|---|---|---|---|---|
| $f_{10}$ | 1.16 | 2.32 | CP1 | 1.174 | 1.124 | 1.21% | 3.10% |
| | | | CP2 | 2.331 | 2.372 | 0.47% | 2.24% |
| | | | CP3 | 1.183 | 1.124 | 1.98% | 3.10% |
| $f_{20}$ | 1.93 | 3.86 | CP1 | 1.987 | 1.873 | 2.95% | 2.35% |
| | | | CP2 | 3.889 | 3.870 | 0.75% | 0.26% |
| | | | CP3 | 1.932 | 1.873 | 0.11% | 2.35% |
| $f_{11}$ | 2.09 | 4.18 | CP1 | 2.065 | $N/A$ | 1.20% | $N/A$ |
| | | | CP2 | 4.013 | $N/A$ | 3.99% | $N/A$ |
| | | | CP3 | 1.993 | $N/A$ | 4.64% | $N/A$ |
| $f_{21}$ | 2.38 | 4.76 | CP1 | 2.384 | $N/A$ | 0.17% | $N/A$ |
| | | | CP2 | 4.705 | $N/A$ | 1.16% | $N/A$ |
| | | | CP3 | 2.320 | $N/A$ | 2.52% | $N/A$ |
| $f_{30}$ | 2.44 | 4.88 | CP1 | 2.497 | 2.497 | 2.34% | 2.34% |
| | | | CP2 | 4.897 | 4.869 | 0.35% | 0.23% |
| | | | CP3 | 2.372 | 2.497 | 2.79% | 2.34% |
| $f_{31}$ | 2.70 | 5.40 | CP1 | 2.640 | $N/A$ | 2.22% | $N/A$ |
| | | | CP2 | 5.396 | $N/A$ | 0.07% | $N/A$ |
| | | | CP3 | 2.741 | $N/A$ | 1.52% | $N/A$ |

**Note(s):** *relative error with respect to the analytical (column 2) or imposed (column 3) frequencies; N/A not applicable, only 2D simulations were run

**Table 5.** Comparison of maximum and minimum height waves *[mm]*

| $f_{ij}$ | $\eta_{max}$ Exp. | $\eta_{max}$ Num.* | $\eta_{min}$ Exp. | $\eta_{min}$ Num.* |
|---|---|---|---|---|
| $f_{10}$ | $50.39 \pm 0.35$ | $55.24 \pm 3.73$ | $-25.72 \pm 1.06$ | $-27.59 \pm 0.96$ |
| $f_{20}$ | $22.19 \pm 3.20$ | $26.18 \pm 0.78$ | $-17.52 \pm 4.04$ | $-18.45 \pm 0.56$ |
| $f_{11}$ | $42.44 \pm 0.26$ | $N/A$ | $-30.85 \pm 0.22$ | $N/A$ |
| $f_{21}$ | $19.35 \pm 0.16$ | $N/A$ | $-16.98 \pm 0.20$ | $N/A$ |
| $f_{30}$ | $22.82 \pm 0.10$ | $20.69 \pm 0.88$ | $-16.96 \pm 0.08$ | $-14.57 \pm 0.55$ |
| $f_{31}$ | $24.78 \pm 0.28$ | $N/A$ | $-20.74 \pm 0.20$ | $N/A$ |

**Note(s):** N/A not applicable, only 2D simulations were run. *numerical values with external mass correction

according to our results, this source of error needs to be addressed by adjusting the elevation of the free surface to compensate for the creation or loss of mass.

PFEM was employed in its standard form, using the classic alpha-shape remeshing strategy, and in 2D. The perspectives of this work include extending the simulation to the 3D case, testing recent remeshing algorithms developed for PFEM, and studying the effect of more advanced time integration schemes in PFEM, with the goal of improving both the understanding of sloshing in tanks and the reliability of PFEM simulations.

## References

Ayiehfor, C.M. (2024), "The effects of fluid sloshing on different baffle configurations in storage tanks transported on trucks during an emergency braking", *Open Journal of Fluid Dynamics*, Vol. 14 No. 1, pp. 24-63.

Battaglia, L., López, E.J., Cruchaga, M.A., Storti, M.A. and D'Elía, J. (2022), "Mesh-moving arbitrary Lagrangian–Eulerian three-dimensional technique applied to sloshing problems", *Ocean Engineering*, Vol. 256, p. 111463.

Battaglia, L., Cruchaga, M., Storti, M., D'elía, J., Núñez Aedo, J. and Reinoso, R. (2018), "Numerical modelling of 3D sloshing experiments in rectangular tanks", *Applied Mathematical Modelling*, Vol. 59, pp. 357-378.,

Cai, Z., Topa, A., Djukic, L.P., Herath, M.T. and Pearce, G.M. (2021), "Evaluation of rigid body force in liquid sloshing problems of a partially filled tank: traditional CFD/SPH/ALE comparative study", *Ocean Engineering*, Vol. 236, p. 109556.

Cao, X., Tao, L., Zhang, A.-M. and Ming, F. (2019), "Smoothed particle hydrodynamics (SPH) model for coupled analysis of a damaged ship with internal sloshing in beam seas", *Physics of Fluids*, Vol. 31 No. 3.

Caron, P., Cruchaga, M. and Larreteguy, A. (2018), "Study of 3D sloshing in a vertical cylindrical tank", *Physics of Fluids*, Vol. 30 No. 8.

Castillo, E., Cruchaga, M.A., Baiges, J. and Flores, J. (2019), "An oil sloshing study: adaptive fixed-mesh ALE analysis and comparison with experiments", *Computational Mechanics*, Vol. 63 No. 5, pp. 985-998.

Cerquaglia, M.-L., Thomas, D., Boman, R., Terrapon, V. and Ponthot, J.-P. (2019), "A fully partitioned Lagrangian framework for FSI problems characterized by free surfaces, large solid deformations and displacements, and strong added-mass effects", *Computer Methods in Applied Mechanics and Engineering*, Vol. 348, pp. 409-442.

Cremonesi, M., Franci, A., Idelsohn, S. and Oñate, E. (2020), "A state of the art review of the particle finite element method (PFEM)", *Archives of Computational Methods in Engineering*, Vol. 27 No. 5, pp. 1709-1735.,

Cruchaga, M.A., Ferrada, C., Márquez, N., Osses, S., Storti, M. and Celentano, D. (2016a), "Modeling the sloshing problem in a rectangular tank with submerged incomplete baffles", *International Journal of Numerical Methods for Heat and Fluid Flow*, Vol. 26 Nos 3-4, pp. 722-744.

Cruchaga, M.A., Celentano, D.J. and Tezduyar, T.E. (2009), "Computational modeling of the collapse of a liquid column over an obstacle and experimental validation", *Journal of Applied Mechanics*, Vol. 76 No. 2, p. 21202.

Cruchaga, M., Celentano, D. and Tezduyar, T. (2001), "A moving lagrangian interface technique for flow computations over fixed meshes", *Computer Methods in Applied Mechanics and Engineering*, Vol. 191 Nos 6-7, pp. 525-543.,

Cruchaga, M., Battaglia, L., Storti, M. and D'Elía, J. (2016b), "Numerical modeling and experimental validation of free surface flow problems", *Archives of Computational Methods in Engineering*, Vol. 23 No. 1, pp. 139-169.,

Cruchaga, M.A., Reinoso, R.S., Storti, M.A., Celentano, D.J. and Tezduyar, T.E. (2013), "Finite element computation and experimental validation of sloshing in rectangular tanks", *Computational Mechanics*, Vol. 52 No. 6, pp. 1301-1312.

Falla, R., Bobach, B.-J., Boman, R., Ponthot, J.-P. and Terrapon, V.E. (2023), "Mesh adaption for two-dimensional bounded and free-surface flows with the particle finite element method", *Computational Particle Mechanics*, Vol. 10 No. 5, pp. 1049-1076.,

Fernández, E., Février, S., Lacroix, M., Boman, R. and Ponthot, J.-P. (2023b), "Generalized-$\alpha$ scheme in the pfem for velocity-pressure and displacement-pressure formulations of the incompressible navier–stokes equations", *International Journal for Numerical Methods in Engineering*, Vol. 124 No. 1, pp. 40-79.

Fernández, E., Février, S., Lacroix, M., Boman, R., Papeleux, L. and Ponthot, J.-P. (2023a), "A particle finite element method based on level–set functions", *Journal of Computational Physics*, Vol. 487, p. 112187.

Fernández, E., Lacroix, M., Février, S., Zhang, T., Papeleux, L., Bobach, B.-J., Boman, R., Ryelandt, S., Simar, A. and Ponthot, J.-P. (2024), "Modelling melt Pool dynamics in aluminium-to-steel welds

performed by friction melt bonding: a challenge addressed with the particle finite element method", *Computational Particle Mechanics*, pp. 1-17.

Frandsen, J. and Borthwick, A. (2003), "Simulation of sloshing motions in fixed and vertically excited containers using a 2-D inviscid $\sigma$-transformed finite difference solver", *Journal of Fluids and Structures*, Vol. 18 No. 2, pp. 197-214.

Frandsen, J.B. (2004), "Sloshing motions in excited tanks", *Journal of Computational Physics*, Vol. 196 No. 1, pp. 53-87.

Gimenez, J.M., Ramajo, D.E., Marquez Damian, S., Nigro, N.M. and Idelsohn, S.R. (2017), "An assessment of the potential of PFEM-2 for solving long real-time industrial applications", *Computational Particle Mechanics*, Vol. 4 No. 3, pp. 251-267.

Godderidge, B., Turnock, S., Tan, M. and Earl, C. (2009), "An investigation of multiphase CFD modelling of a lateral sloshing tank", *Computers and Fluids*, Vol. 38 No. 2, pp. 183-193.

Gotoh, H., Khayyer, A., Ikari, H., Arikawa, T. and Shimosako, K. (2014), "On enhancement of incompressible SPH method for simulation of violent sloshing flows", *Applied Ocean Research*, Vol. 46, pp. 104-115.

Grotle, E.L. and Æsøy, V. (2018), "Dynamic modelling of the thermal response enhanced by sloshing in marine lng fuel tanks", *Applied Thermal Engineering*, Vol. 135, pp. 512-520.

Ibrahim, R.A. (2005), *Liquid Sloshing Dynamics: theory and Applications*, Cambridge University Press.

Idelsohn, S.R., Oñate, E. and Pin, F.D. (2004), "The particle finite element method: a powerful tool to solve incompressible flows with free-surfaces and breaking waves", *International Journal for Numerical Methods in Engineering*, Vol. 61 No. 7, pp. 964-989.

Idelsohn, S.R., Marti, J., Becker, P. and Oñate, E. (2014), "Analysis of multifluid flows with large time steps using the particle finite element method", *International Journal for Numerical Methods in Fluids*, Vol. 75 No. 9, pp. 621-644.

Jahanbakhsh, E., Panahi, R. and Seif, M. (2007), "Numerical simulation of three-dimensional interfacial flows", *International Journal of Numerical Methods for Heat and Fluid Flow*, Vol. 17 No. 4, pp. 384-404.

Jiang, S.-C., Teng, B., Bai, W. and Gou, Y. (2015), "Numerical simulation of coupling effect between ship motion and liquid sloshing under wave action", *Ocean Engineering*, Vol. 108, pp. 140-154.

Li, H., Zhang, X. and Yang, X. (2024), "Numerical study of liquid sloshing using smoothed particle hydrodynamics with adaptive spatial resolution", *Engineering Analysis with Boundary Elements*, Vol. 159, pp. 272-287.

Li, L., Hamamoto, Y., Liu, Y. and Zhang, X. (2014), "Sloshing impact simulation with material point method and its experimental validations", *Computers and Fluids*, Vol. 103, pp. 86-99.,

Liu, D., Cai, Q., Li, Y., He, Y. and Wang, J. (2025), "Experimental study of primary-and higher-mode resonant sloshing in a horizontally excited square-base tank", *Applied Ocean Research*, Vol. 156, p. 104482.

Núñez Aedo, J., Cruchaga, M.A. and Storti, M.A. (2024), "A numerical and experimental study of a buoy interacting with waves", *International Journal of Numerical Methods for Heat and Fluid Flow*, Vol. 34 No. 1, pp. 280-308.

Núñez Aedo, J., Cruchaga, M. and Castillo del Barrio, E. (2020), "Study on the dependence with the filling level of the sloshing wave pattern in a rectangular tank", *Physics of Fluids*, Vol. 32 No. 1, p. 12101.

Oñate, E., Idelsohn, S.R., Del Pin, F. and Aubry, R. (2004), "The particle finite element method—an overview", *International Journal of Computational Methods*, Vol. 1 No. 2, pp. 267-307.

Pizzoli, M., Saltari, F., Coppotelli, G. and Mastroddi, F. (2023), "Neural network-based reduced-order modeling for nonlinear vertical sloshing with experimental validation", *Nonlinear Dynamics*, Vol. 111 No. 10, pp. 8913-8933.,

Rafiee, A., Pistani, F. and Thiagarajan, K. (2011), "Study of liquid sloshing: numerical and experimental approach", *Computational Mechanics*, Vol. 47 No. 1, pp. 65-75.

Saltari, F., Pizzoli, M., Coppotelli, G., Gambioli, F., Cooper, J.E. and Mastroddi, F. (2022), "Experimental characterisation of sloshing tank dissipative behaviour in vertical harmonic excitation", *Journal of Fluids and Structures*, Vol. 109, p. 103478.

Siraye, W., Wakjira, A. and Nallamothu, R.B. (2023), "An analysis of fuel oil sloshing in partially filled cargo tanker trucks under cornering conditions using various baffle systems", *Journal of Engineering*, Vol. 2023 No. 1, p. 9941864.

Yang, C., Niu, R. and Zhang, P. (2021), "Numerical analyses of liquid slosh by finite volume and lattice boltzmann methods", *Aerospace Science and Technology*, Vol. 113, p. 106681.

Yvonnet, J., Quang, H.L. and He, Q.-C. (2008), "An XFEM/level set approach to modelling surface/interface effects and to computing the size-dependent effective properties of nanocomposites", *Computational Mechanics*, Vol. 42 No. 1, pp. 119-131.

Zhang, G-y., Zhao, W-W. and Wan, D-C (2022), "Numerical simulations of sloshing waves in vertically excited square tank by improved MPS method", *Journal of Hydrodynamics*, Vol. 34 No. 1, pp. 76-84.

**Corresponding author**
Marcela A. Cruchaga can be contacted at: marcela.cruchaga@usach.cl